Retrieval of Cirrus Optical Thickness and Assessment of Crystal Shape from Ground-Based Imaging Spectrometry

M. Schäfer, E. Bierwirth, A. Ehrlich, F. Heyner and M. Wendisch

Abstract

An imaging spectrometer (AisaEAGLE) is applied for ground-based measurements of downward spectral radiance fields with high spatial (1024 spatial pixels within 36.7° field of view), spectral (488 spectral pixels, 400-970 nm, 1.25 nm full width at half maximum) and temporal (4-30 Hz) resolution. The calibration, measurement, and data evaluation procedures are introduced. A method is presented that retrieves the cirrus optical thickness τ_{ci} using the spectral radiance data collected by AisaEAGLE. On the basis of four measurement cases during the second campaign of the Cloud Aerosol Radiation and tuRbulence of trade wInd cumuli over BArbados (CARRIBA) project in 2011 the spatial inhomogeneity of the investigated cirrus is characterized by the standard deviation of the retrieved τ_{ci}, as well as the width of the frequency distribution of the retrieved τ_{ci}. By comparing measured and simulated downward solar radiances as a function of scattering angle, a first estimation of the detected cirrus ice crystal shape is given and used in the retrieval of $\tau_{ci.}$

Zusammenfassung

Ein abbildendes Spektrometer (AisaEAGLE) wurde bodengebunden zur Messung von Feldern abwärts gerichteter spektraler Strahldichten mit hoher räumlicher (1024 Raumpixel auf 36.7° FOV), spektraler (488 spektrale Pixel, 400-970 nm, 1.25 nm FWHM) und zeitlicher (4-30 Hz) Auflösung verwendet. Die Kalibrierungsprozedur, das Messverfahren sowie die Datenauswertung werden hier vorgestellt. Weiter wird eine Methode zur Ableitung der Zirrus optischen Dicke τ_{ci} unter Verwendung dieser bodengebundenen spektralen Strahldichtedaten vorgestellt. Auf der Grundlage von vier Messzeiträumen während der zweiten Kampagne des Cloud Aerosol Radiation and tuRbulence of trade wInd cumuli over BArbados (CARRIBA) Projektes in 2011 wird die räumliche Inhomogenität der untersuchten Zirren durch die Standardabweichung der abgeleiteten τ_{ci}, wie auch der Breite ihrer Häufigkeitsverteilungen charakterisiert. Vergleiche der gemessenen Strahldichten mit Simulationen abwärts gerichteter solarer Strahldichten als Funktion der Streuwinkel ermöglichen eine erste Abschätzung der Eiskristallform im detektierten Zirrus und gehen in die Ableitung der τ_{ci} ein.

1. Introduction

Satellite-derived cirrus cloud climatology includes cloud cover, optical thickness, and crystal effective radius. Changing either of those parameters may change the magnitude of their radiative forcing. For example, in current global circulation models a standard value of 25 µm for ice crystal effective radius is assumed. For slightly smaller crystals, cirrus clouds would have a stronger cooling effect (Garrett et al., 2003). However, cirrus clouds often show a high spatial and temporal variability and in addition might be optically thin. This partly makes it hard to detect cirrus by common remote sensing techniques. The microphysical composition adds a further complication. Depending on crystal shape, the cloud radiative properties may vary substantially and cause biases in both satellite retrievals (based on reflected radiance, Eichler et al., 2009) and the energy budget (related to irradiance, Wendisch et al., 2005, 2007).

Passive satellite imaging spectroradiometers used for cloud retrievals measure the radiance field emerging from clouds. The applicability of those data for remote sensing is limited by radiative smoothing and other 3D effects, but also by the limited number of wavelength bands and spatial resolution of the sensor. A second source of uncertainty in cirrus retrievals arises from the forward simulation applied within the retrieval algorithm. In the special case of ice clouds, assumptions about the crystal shape and the corresponding scattering properties are made. Eichler et al. (2009) showed that these assumptions can add an uncertainty of up to 70% and 20% in optical thickness and effective radius, respectively. A way to check the retrieval algorithms with respect to both horizontal cloud heterogeneity and resolution and to crystal shape is provided by flying airborne versions of spectroradiometers above cirrus clouds, such as the MAS (MODIS Airborne Simulator).

Along with extensive microphysical and solar radiation instruments as well as radiative transfer simulations Schmidt et al. (2007) and Eichler et al. (2009) investigated the differences between retrieved and measured microphysical cloud properties. Schmidt et al. (2007) revealed large gaps between retrieved effective radius from MAS and simultaneous in situ measurements. This disagreement is probably related to the often discussed enhanced absorption and has not been resolved yet, partly because it has been extremely difficult to collocate remote sensing above the clouds and concurrent in-cloud microphysical measurements. Such experiments are extremely important to link satellite cloud observations of coarse resolution to spatially highly resolved measurements of cloud properties. Unfortunately, such experiments are rare, partly because instruments like MAS are very complex and expensive and are not available for frequent cloud experiments.

Furthermore, the modeling of cirrus inhomogeneities has to be improved. There are only very few cloud-resolving model studies on cirrus inhomogeneities, with regard to the radiative impact on the structure of cirrus clouds (Dobbie and Jonas, 2001), turbulence effects (Liu et al., 2003), or shear instabilities (Marsham and Dobbie, 2003). For a realistic simulation a high spatial and temporal resolution is required to represent the small scale features of cirrus inhomogeneities. In this regard, ground-based imaging spectrometers are a helpful tool to provide information on the cirrus heterogeneity in terms of field of radiance and cirrus optical thickness.

Within this study a ground-based spectral imager (AisaEAGLE Hanus et al., 2008) is applied to measure downward spectral radiance fields with high spatial (1024 spatial pixels within 36.7° field of view, FOV), spectral (488 spectral pixels, 400-970 nm, 1.25 nm full width at half maximum, FWHM) and temporal (4-30 Hz) resolution. Commonly AisaEAGLE is used for airborne observations of the Earth's surface and upward spectral radiance. In this paper AisaEAGLE is applied on the ground to measure downward solar radiances. In Section 2 the AisaEAGLE is technically characterized and its calibration and data evaluation procedures are described and exemplified. Section 3 introduces a new method to retrieve the cirrus optical thickness (τ_{ci}) from spectral radiance data, which also uses angular sampling of the phase function to obtain information about the particle shape. Its application to measurements is presented in Section 4.

2. Measurements of Spectral Radiance Fields

2.1 Campaign and Measurement Site

In April 2011, directional and spectral measurements of downward solar radiance were performed with the spectral imager AisaEAGLE on Barbados during the second campaign of the Cloud Aerosol Radiation and tuRbulence of trade wInd cumuli over BArbados (CARRIBA) project (Siebert et al., 2012). The aim of CARRIBA was to investigate microphysical and radiative processes within and next to shallow trade wind cumuli by helicopter-borne and ground-based observations (e.g., Werner et al., 2012). However, also cirrus clouds have frequently been observed by the ground-based instrumentation.

During the CARRIBA project in 2011, the imaging spectrometer AisaEAGLE was located in the Barbados Cloud Observatory (BCO) of the Max Planck Institute for Meteorology (Hamburg, Germany) at Deebles Point (13.15° N, 59.42° W), a cape at the east coast of Barbados.

Additionally, measurements with a Raman LIDAR and a cloud RADAR as well as radiosonde launches are available. See Siebert et al. (2012) for a more detailed description of the BCO. In parallel to the AisaEAGLE radiance measurements, all-sky images were collected every 15 seconds to receive information about the cloud situation (cloud coverage, cloud type, heading).

Downward spectral radiance was measured under inhomogeneous cloud cover on 14 different days. Each day, two hours of data were collected coordinated with the helicopter-borne measurements. In the following, four cases with measurements below cirrus and without low cumuli clouds were evaluated.

2.2 Imaging Spectrometer AisaEAGLE

The AisaEAGLE is a commercial imaging spectrometer which is manufactured by Specim Ltd. in Finland (Hanus et al., 2008). It is a single-line sensor with 1024 spatial pixels. The instrument measures radiances in three dimensions: space, time, and wavelength. The spatial and spectral dimensions are resolved by a special set of optics that displays the image onto a two-dimensional (2D) sensor chip. The third dimension, time, corresponds to the motion of the clouds passing over the sensor. An optical

schematic for the path of the electromagnetic radiation detected by the center spatial pixel is shown in Figure 1.

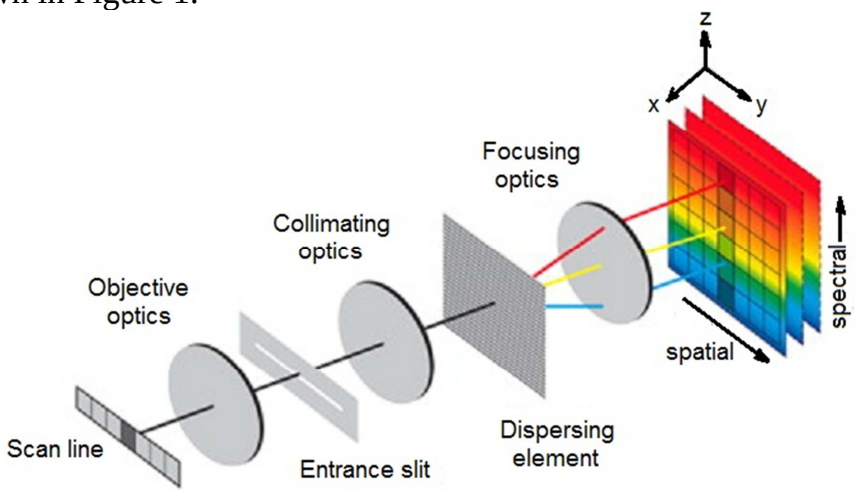

Fig. 1: Optical scheme of an imaging spectrometer. The figure is adapted from DellEndice et al. (2009).

The incoming solar radiation within the field of view (FOV) of AisaEAGLE is collected by a lens and an entrance slit. A collimating optics direct the radiation to a grating (dispersing element) where it is split into its spectral components. The spectral components are focused on the detector which consists of a charge-coupled device (CCD) element for the spatial and spectral dimensions.

In contrast to airborne measurements (Bierwirth et al., 2012), the 2D image evolves from the cloud movement and not from the sensor movement. The sensor was aligned perpendicularly to the direction of the cloud movement, thus 2D images of clouds with high spatial resolution are obtained. The FOV of the AisaEAGLE depends on the lens that is used for the measurements. During the CARRIBA project in 2011, a lens with an opening angle of about 36.7° was mounted.

While the swath increases with distance to the cloud by the tangent of the opening angle, the pixel size depends on its position on the sensor line. The FOV of a pixel (pixel width) in the center (viewing zenith) is smaller than that of a pixel at the edge. The "time" dimension of the spectral data set also translates to a spatial quantity: the length l_{pixel} of the FOV of a pixel is the product of the perpendicular cloud velocity v_{cloud} and the selected integration time t_{int} for the measurement. Considering additionally for a non-perfect perpendicular orientation with the angle α between the flow direction of the cirrus and the orientation of the sensor line, l_{pixel} is then given by:

$$l_{pixel} = |\sin\alpha| \cdot v_{cloud} \cdot t_{int} \qquad (1)$$

Figure 2 illustrates the measurement geometry which is needed to derive the detected scattering angles ϑ for each spatial pixel. The scattering angle ϑ is derived by the scalar product between the vector of the incoming solar radiation (SC) and the vector of the radiation scattered into the sensor direction (CD):

$$\cos\vartheta = \frac{\overrightarrow{CD}\cdot\overrightarrow{SC}}{|\overrightarrow{CD}|\cdot|\overrightarrow{SC}|} = \cos\varphi_0 \sin\theta_0 \sin\beta_i + \cos\theta_0 \cos\beta_i \qquad (2)$$

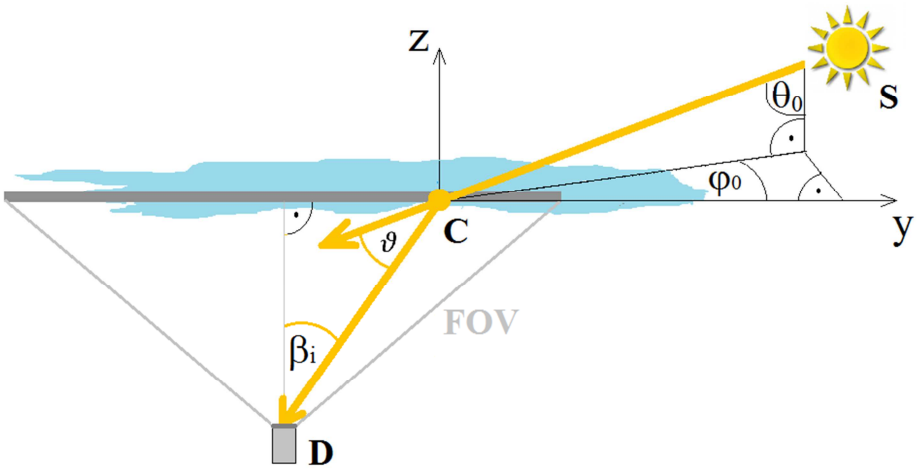

Fig. 2: Illustration of the AisaEAGLE measurement geometry in a Cartesian coordinate system (x, y, z) with position of the Sun (S), a scattering cloud particle (C) and the AisaEAGLE detector (D). θ_0 is the solar zenith angle, φ_0 the solar azimuth angle, ϑ the scattering angle, and β_i the viewing angle of the corresponding pixel.

For the calculations the solar azimuth angle φ is considered relatively to the azimuth angle of the AisaEAGLE sensor line. Therefore, φ is cancelled out in the above given equation for the scattering angle ϑ.

For each spatial pixel the radiance is measured spectrally between 400 nm and 970 nm with 488 wavelength pixels. The spectral resolution is 1.25 nm FWHM. During the CARRIBA project in 2011 a frame rate of 4 Hz was used. The integration time was chosen between 10 ms and 30 ms, depending on the illumination of the cloud scene.

2.3 Calibration, Corrections, and Data Handling

The data collected by the AisaEAGLE are given in counts per integration time. A calibration to obtain radiances I in units of $W\,m^{-2}\,nm^{-1}\,sr^{-1}$ is performed with an integrating sphere and the software AisaTools (provided by the manufacturer). The dark current is determined separately with a shutter. The calibration factors for each pixel are calculated from the calibration measurements using a certified radiance standard (integrating sphere) traceable to the U. S. National Institute of Standards and Technology.

Since the AisaEAGLE detector is based on CCD technique, it is necessary to correct for the smear effect in calibration and measurement data. The smear effect occurs during the read-out process of the collected photo-electrons which are shifted step by step from one spectral pixel to the neighboring one into the direction of the read-out unit. The read-out process is not infinitely fast. Due to the fact that radiation still can reach the sensor during the read-out, the pixels are contaminated by an additional signal. The read-out process for the longer wavelengths ends earlier than the read-out for the shorter wavelengths. Therefore, the additional signal (smear effect) is larger for shorter wavelengths which are longer illuminated during the read-out. The whole procedure for correcting the measurements for the smear effect can be found in Schäfer et al. (2013).

3. Retrieval of Cirrus Optical Thickness

For the retrieval of the cirrus optical thickness τ_{ci} from the measured downward spectral radiance $I^{\downarrow}$ transmitted through the cirrus, radiative transfer calculations were performed. The radiative transfer solver DISORT 2 (Discrete Ordinate Radiative Transfer) was applied. Input parameters, such as cloud optical properties, aerosol content and spectral surface albedo are provided by the library for radiative transfer calculations (libRadtran, Mayer and Kylling, 2005). The so called HEY (Hong, Emde, Yang) parameterization was used to describe the scattering properties of ice crystals. It uses pre-calculated ice cloud optical properties including full phase matrices generated with the models by Yang et al. (2000)

The simulations were performed for 530 nm wavelength, which allows a comparison with the available LIDAR data. Since the BCO is located at the far end of this cape, the measurement site is surrounded by half water and half rocks and grass. For simplification the surface albedo in the radiative transfer simulations was assumed to be only water, as derived by Wendisch et al. (2004) providing a value of 0.068. A maritime aerosol type, provided by libRadtran was used. The cloud altitude and cloud vertical extend was determined by LIDAR measurements of BCO. On the basis of the MODIS data collection 5, a fixed effective radius (r_{eff}) of 20 µm was assumed as no direct retrieval from AisaEAGLE is possible. Downward solar radiance $I^{\downarrow}_{cal}$ was calculated as a function of τ_{ci}. By fitting the measured downward solar radiance $I^{\downarrow}_{meas}$ to the simulation, the corresponding τ_{ci} is interpolated.

The imaging measurements require an accurate description of the sensor geometry in the simulations as shown in Figure 2. The sensor was aligned horizontally. The viewing zenith angle is given by the sensor FOV ($\beta = \pm 18°$). Related to this range, the downward solar radiance $I^{\downarrow}_{cal}$ was calculated in steps of 0.3°.

4. Measurements

4.1 Measurement Cases

Four datasets of different days were evaluated: 9, 16, 18, and 23 April 2011. Figure 3a to 3d show all-sky images from the beginning of the four cases. These days showed persistent cirrus with no other clouds below. An overview of the main characteristics of the evaluated measurement periods can be found in Table 1.

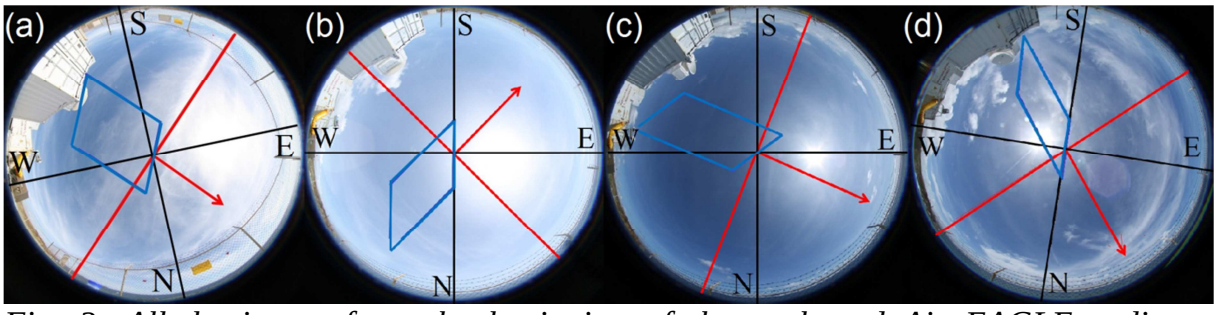

Fig. 3: All-sky image from the beginning of the evaluated AisaEAGLE radiance measurements for (a) 9 April 2011 (b) 16 April 2011 (c) 18 April 2011 (d) 23 April 2011. In each image the arrow indicates the heading of the cirrus and the rhomb indicates the FOV of the AisaEAGLE radiance measurement.

Tab. 1: Characteristics of the evaluated measurement periods

	9th April	16th April	18th April	23rd April
start time (UTC)	13:26	13:43	13:43	16:45
average Θ_0 (°)	36.7	28.6	28.5	14.5
heading	SW → NW	NW → SW	WSW → ESE	SSW → NNE
appearance	inhomog.	homog.	homog.	inhomog.
cloud height (km)	11 – 15	12 – 15	13 – 15	11 – 14
$\bar{I}^{\downarrow}$ (W m^{-2} nm^{-1} sr^{-1}) ± σ	0.08 ± 0.02	0.11 ± 0.02	0.10 ± 0.03	0.16 ± 0.03
τ_{ci} ± σ	0.41 ± 0.17	0.28 ± 0.09	0.20 ± 0.03	0.05 ± 0.04
covered theta range	35.1 – 47.1	32.6 – 37.9	21.2 – 48.2	12.2 – 36.3

The heading was derived by comparing the position of clouds in the sequence of all-sky images (15 s time resolution). The blue box indicates the area covered by the AisaEAGLE radiance measurements, the area of cirrus which is heading across the sensor line during the measurement period. Due to the fact that the AisaEAGLE was not orientated perfectly in perpendicular direction of the cirrus heading, the covered area is not a rectangle in most cases.

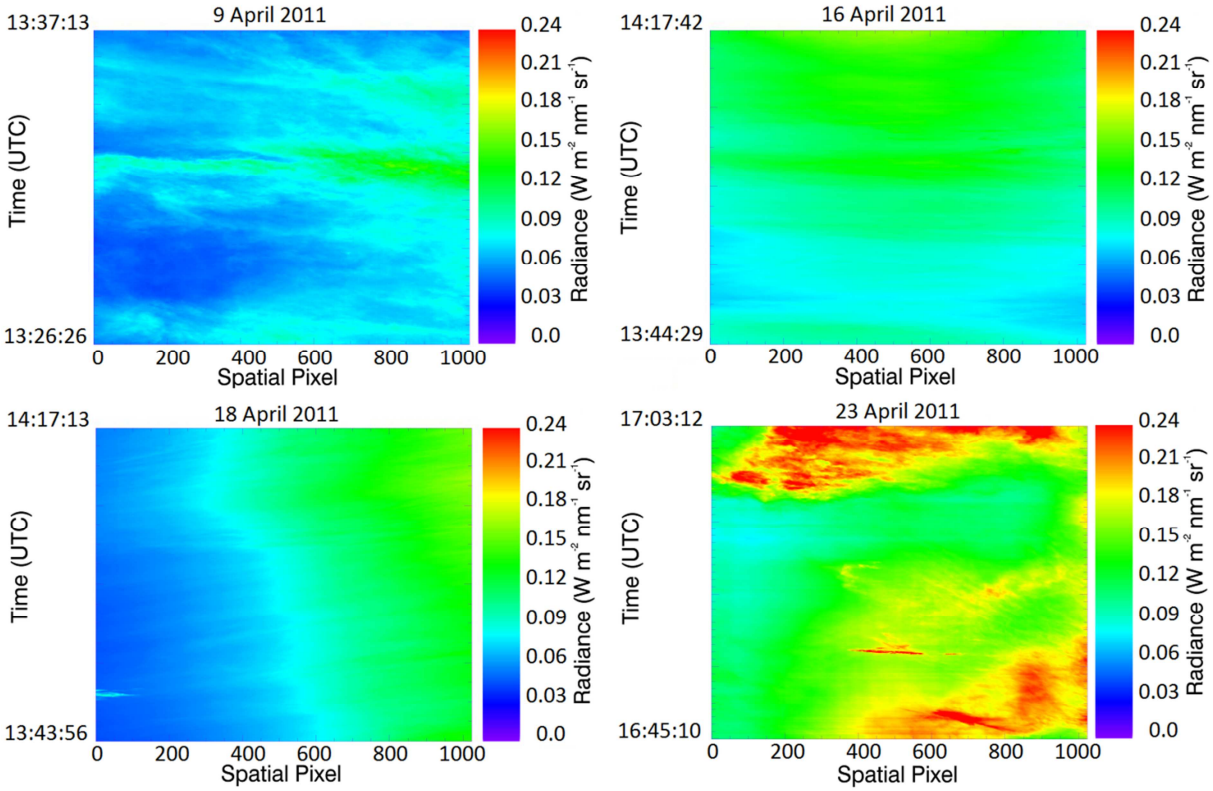

Fig. 4: 2D images of the evaluated AisaEAGLE radiance measurements at 530 nm with the measured $I^{\downarrow}$ (W m^{-2} nm^{-1} sr^{-1}) given in colour scales.

The cirrus for 16 and 18 April 2011 were quit homogeneous. On 9 and 23 April 2011, rather inhomogeneous cirrus was observed. On the 23 April 2011, a 22° halo was identified on the all-sky images but did not range into the FOV of AisaEAGLE.

Fields of transmitted downward radiance $I^{\downarrow}$ as measured by AisaEAGLE for the four cases are presented in Figure 4. The radiance is given for 530 nm in two-dimensional colour scale images for all 1024 spatial pixels on the abscissa and the time

of measurement on the ordinate. The cloud structure seen in the all-sky images in Figures 3a to 3d is clearly imprinted in the radiance field. The average values $\bar{I}^{\downarrow}$ of the measured radiance $I^{\downarrow}$ are given in Table 1. The highest value of $\bar{I}^{\downarrow}$ was observed for 23 April 2011 and the lowest for 9 April 2011.

Especially for 18 April 2011 it is evident that the image is getting brighter from the left to the right side. During this day the sensor line of AisaEAGLE was orientated from north-west (pixel 1) to south-east (pixel 1024) while the solar azimuth position was in the East at the same time. This brightening is caused by enhanced scattering for small scattering angles, corresponding to the shape of the scattering phase function of ice crystals. Therefore, while performing the radiative transfer calculations to retrieve τ_{ci} it is necessary to know the exact alignment of the sensor line and the exact position of the Sun. If the sensor orientation is carefully considered, the retrieval will account for this brightness effect caused by enhanced forward scattering of ice crystals. Using the calculated scattering angles derived for each spatial pixel from Equation 2, Figure 4 can be displayed as a function of scattering angle as shown in Figure 5.

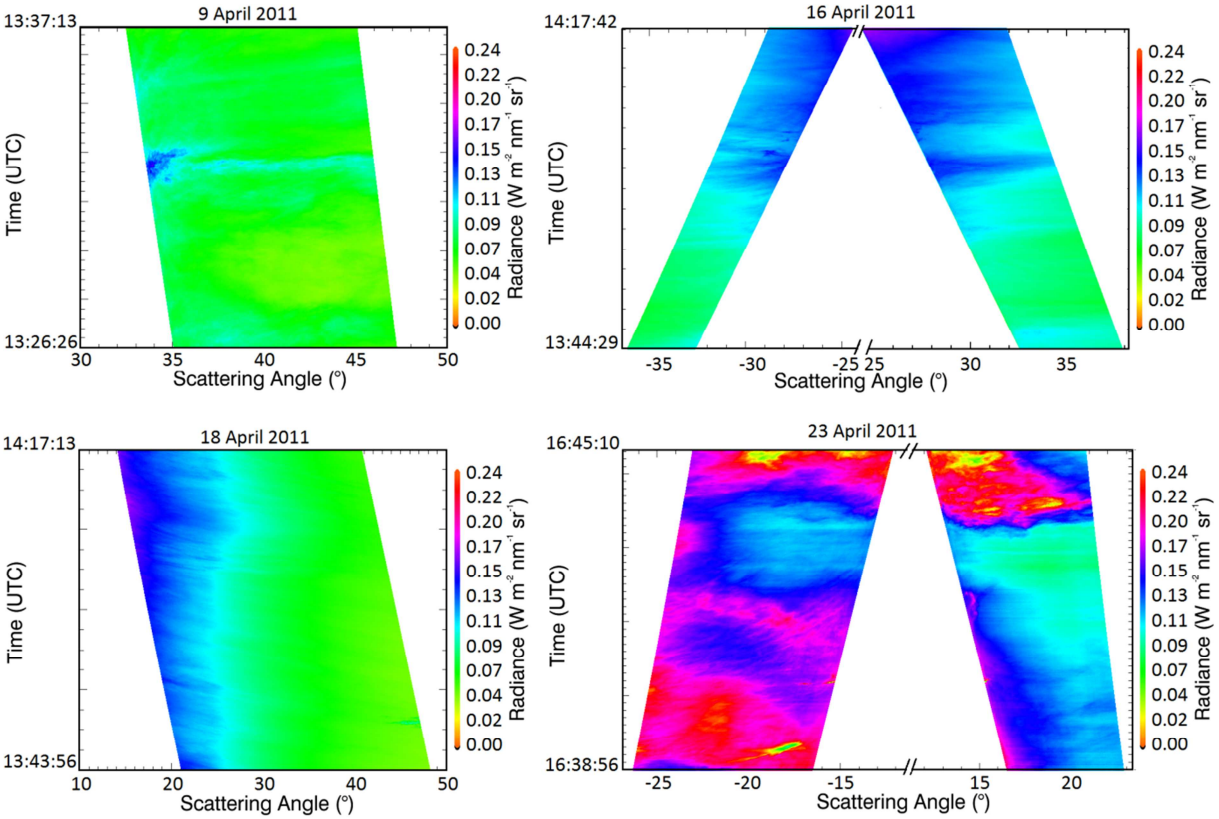

Fig. 5: Time series of the measured downward solar radiance $I^{\downarrow}$ during the four measurement cases as a function of scattering angles. The range of the abscissa of each image is fitted to the corresponding range of covered scattering angles.

The scattering angles are symmetrical for each pixel to the pixel closest to the Sun. If the Sun's azimuthal position is almost perpendicular to the sensor line, a minimum appears in the detected scattering angles per spatial pixel. In such cases, the plot of $I^{\downarrow}$ as a function of the scattering angle would have overlapping sections. For clarity, one of those sections is assigned a negative sign in Figure 5. Furthermore, because of the Sun's movement during the measurement period, the images are not rectangular any more. The advantage of the illustration using scattering angles is that structures in the

image related to scattering features of the ice crystals occur now in a fixed position throughout the time series as can be seen for 18 April 2011. The radiance always increases with decreasing scattering angle which is a typical characteristic of the forward scatting of ice crystals.

4.2 Retrieved Ice Crystal Shape

With regard to the all-sky image in Figure 3c (18 April 2011), the best estimation for the ice crystal shape should be the assumption of rough aggregates, since no halo can be figured out in this image. Figure 6 shows the averaged downward solar radiance $I^{\downarrow}$ as a function of scattering angles for 18 April. Additionally included are simulations of the downward solar radiance for different values of τ_{ci}.

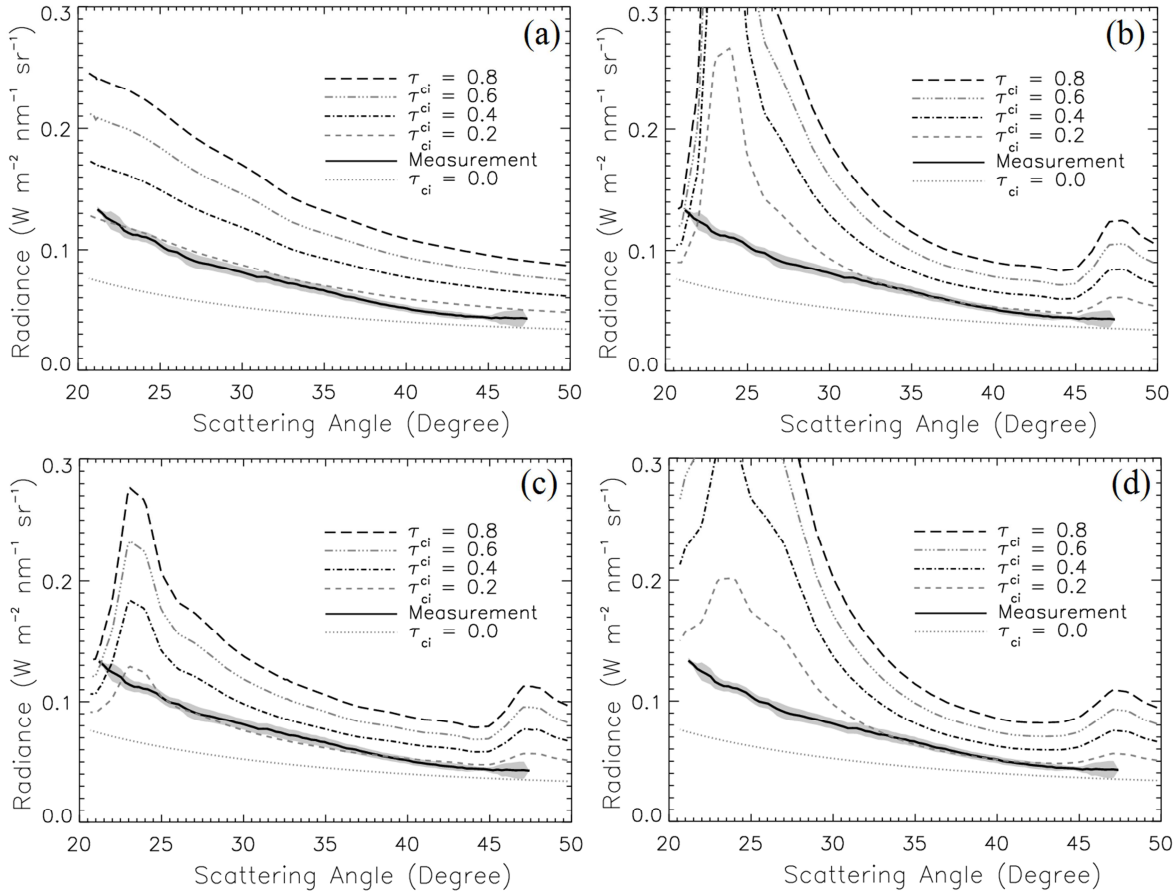

Fig. 6: Measured and simulated $I^{\downarrow}$ as a function of scattering angles. Measurement from 18 April 2011. The standard deviation of the measurement is given as a grey shade. The simulations were performed for different τ_{ci} and assumed ice crystal shapes of a) rough aggregates, b) solid columns, c) plates, and d) mixture.

As can be seen, by performing the simulations for rough aggregates no halo appears in the calculated radiance. However, for the calculations with solid columns, plates, as well as a mixture of ice crystals, the two halo regions are well defined in the simulation results. By comparing the measured downward solar radiance $I^{\downarrow}$ to the simulated ones, the best agreement can be found for rough aggregates. For this reason, in Section 4.3, the τ_{ci} for 18 April 2011 were retrieved by assuming rough aggregates for the ice crystal shape.

As mentioned before, on 23 April 2011 a halo was observed as it can be seen in the all-sky image in Figure 3d. Therefore, in comparison to 18 April 2011 another ice crystal shape than rough aggregates can be expected. Although it is not shown here, between the measured radiance $I^{\downarrow}$ and the simulated one for rough aggregates, only less agreement can be found. For solid columns, plates, and mixed ice crystals it looks more comparable. Since the cloud inhomogeneities during this day were rather high, unfortunately it becomes difficult to figure out the exact ice crystal shape for this case. Therefore, in the following retrieval of the τ_{ci} for 23 April 2011, ice crystals in the shape of solid columns (default setting in libRadtran) were assumed.

Using this method, for 9 April 2011 and 16 April 2011 it is more difficult to estimate the most likely cirrus crystal shape. This is due to the only narrow range of detected scattering angles (halo region is not covered) and the rather high cirrus inhomogeneity on 9 April 2011. Therefore, the radiative transfer calculations to retrieve τ_{ci} were also performed for solid columns.

4.3 Retrieved τ_{ci}

The τ_{ci} retrieved by the presented method are displayed in Figure 7. The unit of the abscissa and ordinate are converted into distances to the swath width and heading distance of the cirrus, respectively. For this, the altitude of the cloud base was used to derive the values for the abscissa. The average wind velocity in the same altitude, derived from the U. S. National Oceanic and Atmospheric Administration (NOAA), was used to convert the ordinate into a distance.

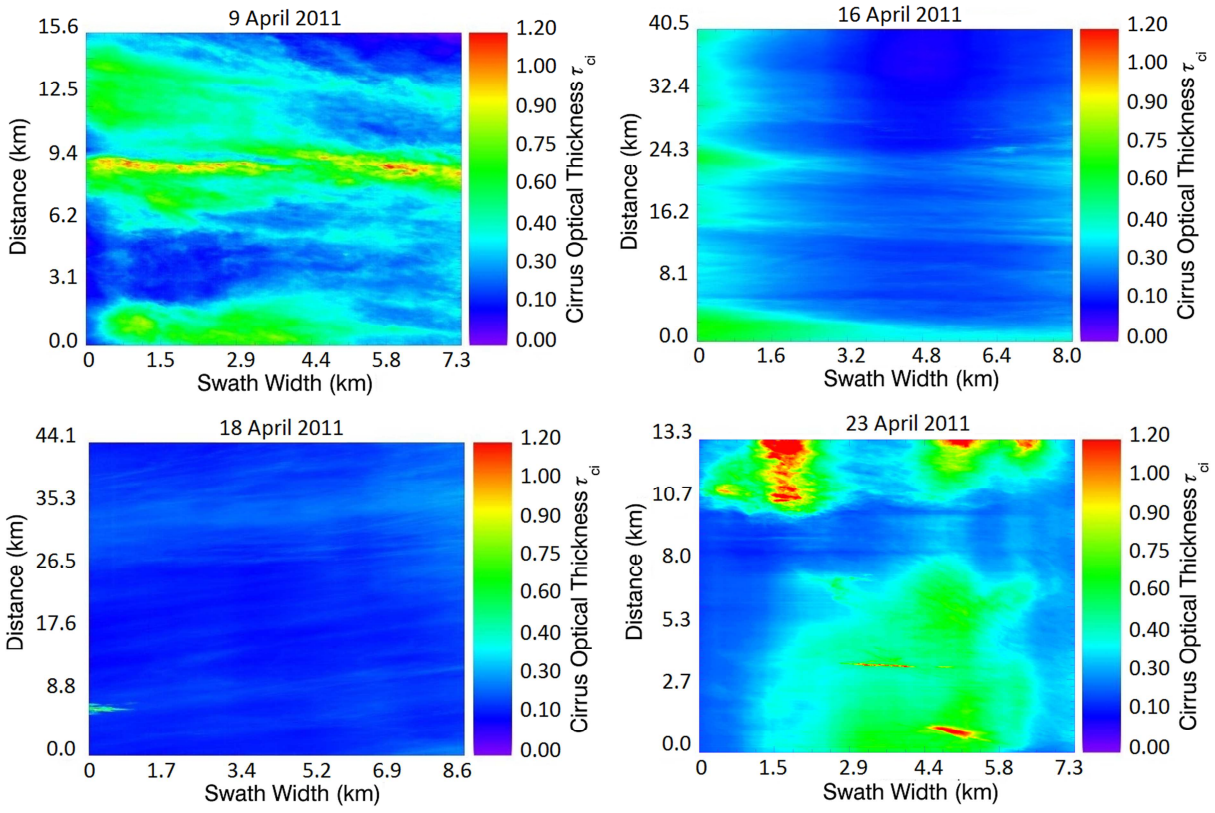

Fig. 7: Time series of the retrieved τ_{ci} during the four measurement case. Abscissa and ordinate values are different due to different measurement conditions.

For 18 April 2011 the retrieved τ_{ci} indicates that the cloud is very homogeneous. This confirms that the observed increase in radiance (Figure 4 and 5) results from enhanced forward scattering of ice crystals and has been considered correctly by the model. For 23 April 2011 it can be found that quite inhomogeneous cirrus was observed with large areas of clear-sky regions in between.

Frequency distributions of the retrieved τ_{ci} for each measurement day are shown in Figure 8. The histograms are normalized by the total of the retrieved τ_{ci} with a bin size of 0.01 in τ_{ci}.

The average values and the standard deviation of the retrieved τ_{ci} for each dataset are listed in Table 1. High standard deviations compared to the average values are a further measure for the inhomogeneities of the detected cirrus. Thus, the AisaEAGLE measurements confirm that the cirrus on 16 and 18 April 2011 was more homogeneous than on 9 and 23 April 2011.

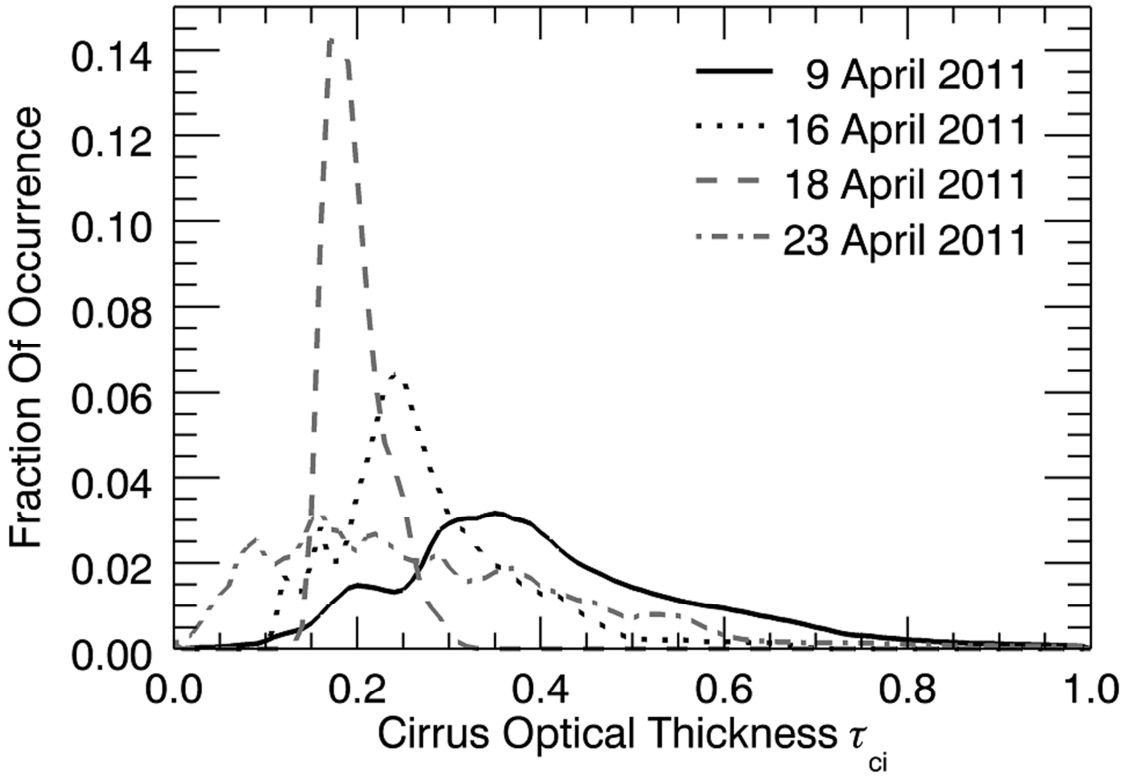

Fig. 8: Normalized histograms of τ_{ci} for each of the four considered measurement days. Bin size is 0.01 in cirrus optical thickness τ_{ci}.

5. Summary and Conclusions

Downward solar radiance fields were measured with high spatial, spectral, and temporal resolution using the imaging spectrometer AisaEAGLE. The procedure of data evaluation (dark current correction, smear correction) was described briefly.

The cirrus optical thickness τ_{ci} is retrieved from the radiance measurements. On the basis of four measurement cases collected during the CARRIBA project in 2011 on Barbados, the feasibility of retrieving cirrus optical thickness at high spatial resolution and characterizing the cirrus heterogeneity was demonstrated. The cirrus on 16 and 18 April 2011 was quite homogeneous with mean τ_{ci} of 0.28 and 0.20 and coefficients of

variation of 0.09 and 0.03. Therefore, the 16 and 18 April 2011 showed quite homogeneous cirrus, while on 9 and 23 April 2011 rather inhomogeneous cirrus with mean τ_{ci} of 0.41 and 0.05 and coefficients of variation of 0.17 and 0.04 was observed. It was found that the inhomogeneity of the investigated cirrus is represented by the standard deviation of the retrieved τ_{ci}.
The determination of the ice crystal shape is complicated without in situ measurements inside the cirrus. Due to the fact that AisaEAGLE is able to measure radiance as a function of a wide range of calculable scattering angle, it gives the opportunity to receive information about the scattering phase function from the radiance measurements. A first feasibility study on this topic was given during this work by comparing measured and simulated radiance as a function of scattering angles. By this, it was already possible to distinguish between halo producing and non-halo producing ice crystal shapes. This topic will be further investigated in future studies by increasing the detected scattering angle range, using a scanning version of the AisaEAGLE, as well as by parameterizing the cirrus inhomogeneities. The results will then be implemented in the retrieval algorithm to allow cirrus retrieval independent on any assumption of ice crystal shape.

To adjust the measurement set up for this purpose, the best way to operate AisaEAGLE in a ground-based application is to adjust the sensor line into the azimuthal direction of the Sun, with the clouds heading perpendicularly across the sensor line. Performing the measurements like this, the maximum possible range of the scattering phase function as well as the maximum possible range of the cloud field can be detected without a spatial distortion of the cloud shape.

6. Outlook

It has been shown that radiance measurements, collected with the imaging spectrometer AisaEAGLE can be used to retrieve the ice crystal shape of the detected cirrus. This holds for measurements where the range of the detected scattering angles is wide enough and reaches into the halo range.

On the basis of this study, the assessment of the ice crystal shape from angular measurements of the solar spectral radiance will be applied to airborne measurements of the AisaEAGLE system. Furthermore, the data analysis will be extended to separate between water and ice clouds. Since the scattering phase functions of cloud droplets and ice crystals are quite different to each other, this will help to identify the cloud particles phase (droplets, ice crystal).

Measurements to test this approach were already performed in April 2012 during the Vertical Distribution of ice in Arctic Clouds (VERDI) project in Canada. Figure 9 shows such airborne measurements. The variable shape of the detected scattering angle range arises from the measurement geometry. Where the detected scattering angle range is wide, the flight direction was perpendicular to the azimuthal position of the Sun. In contrast to this, the detected scattering angle range narrows, when the flight direction was into the direction of the azimuthal position of the Sun or away from it.

For the selected case the range of the scattering angles reaches from 90° to almost 140°. Unfortunately due to this range the halo region (22°, 46°) as well as the cloud-bow region (≈138°) is not covered. The cloud-bow is a backscatter feature,

which is typically for scattering by liquid water droplets. If this cloud-bow appears in the data it would indicate the detected cloud as a liquid water cloud.

During the upcoming Radiative Closure Experiment for Arctic Clouds (RACEPAC) campaign in April/ May 2014 the fly pattern will be adjusted to cover also the missing scattering angle range. This will be done by a perpendicular flight pattern relative to the Sun's azimuthal position. This flight pattern and additional roll manoeuvres will increase the attitude angles of the airplane, which enlarges the range of detectable scattering angles.

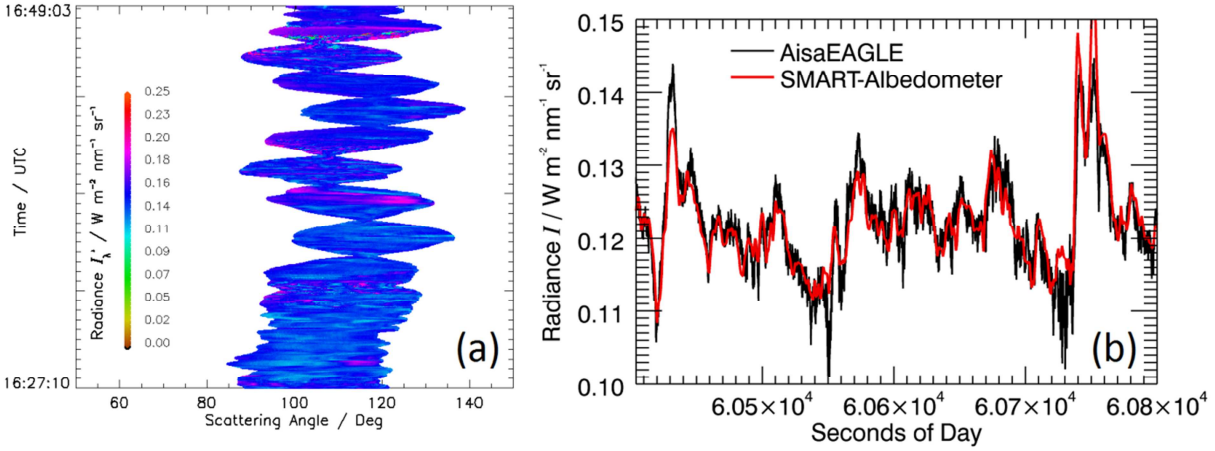

Fig. 9: a) Example time series of radiance measured by AisaEAGLE as a function of scattering angles. b) Example time series of the radiance measured by the center spatial pixel of AisaEAGLE and the SMART-Albedometer.

The results derived by this method will be validated against retrieval results of measurements performed with the Spectral Modular Airborne Radiation measurement sysTem (SMART-) Albedometer (Wendisch et al., 2001). With the SMART-Albedometer cloud microphysical properties such as optical thickness, effective radius, and cloud particle phase can be retrieved. A first comparison of the radiance (at 530 nm wavelength), collected by the AisaEAGLE (center spatial pixel) and the SMART-Albedometer during the VERDI project is given in Figure 9b. The collected radiance given in this time series can be found as well matched.

This new method will extend the information about microphysical properties of the observed two dimensional cloud field while the SMART-Albedometer measures only in Nadir direction. It will allow further investigations concerning the effects of cloud inhomogeneities.

Acknowledgements

We are grateful for funding of project SI 1534/3-1 and WE 1900/18-1 by the German Research Foundation (Deutsche Forschungsgemeinschaft, DFG) within the framework of CARRIBA. The authors thank the Institute for Tropospheric Research, Leipzig, and the Max Planck Institute for Meteorology, Hamburg for organising the campaign and the logistic support at BCO.

References

Bierwirth, E., Ehrlich, A., Wendisch, M., Gayet, J.-F., Gourbeyre, C., Dupuy, R., Herber, A., Neuber, R., and Lampert, A. (2013). Optical thickness and effective radius of Arctic boundary-layer clouds retrieved from airborne nadir and imaging spectrometry. Atmos. Meas. Tech., 6, 1189-1200.

DellEndice, F., Nieke, J., Koetz, B., Schaepman, M. E., and Itten, K. (2009). Improving radiometry of imaging spectrometers by using programmable spectral regions of interest. ISPRS J. Photogramm., 64(6):632 – 639.

Dobbie, S. and Jonas, P. (2001). Radiative influences on the structure and lifetime of cirrus clouds. Q. J. R. Meteorol. Soc., 127:2663–2682.

Eichler, H., Ehrlich, A., Wendisch, M., Mioche, G., Gayet, J.-F., Wirth, M., Emde, C., and Minikin, A. (2009). Influence of ice crystal shape on retrieval of cirrus optical thickness and effective radius: A case study. J. Geophys. Res., 114:D19203, doi:10.1029/2009JD012215.

Garrett, T. J., Gerber, H., Baumgardner, D. G., Twohy, C. H., and Weinstock, E. M. (2003). Small, highly reflective ice crystals in low-latitude cirrus. Geophys. Res. Lett., 30:doi:10.1029/2003GL018153.

Hanus, J., Malenovsky, Z., Homolova, L., Veroslav, K., Petr, L., and Pavel, C. (2008). Potentials of the VNIR Airborne hyperspectral system AISA Eagle. In Symposium GIS Ostrava, (CZ).

Liu, H.-C.,Wang, P., and Schlesinger, R. (2003). A numerical study of cirrus clouds. Part II: Effects of ambient temperature, stability, radiation, ice microphysics, and microdynamics on cirrus evolution. J. Atmos. Sci., 60:1097–1119.

Marsham, J. and Dobbie, S. (2003). The effects of wind shear on cirrus: A large-eddy model and radar case-study. Q. J. R. Meteorol. Soc., 131:2937–2955.

Mayer, B. and Kylling, A. (2005). Technical note: The libRadtran software package for radiative transfer calculations - description and examples of use. Atmos. Chem. Phys., 5:1855–1877.

Schäfer, M., Bierwirth, E., Ehrlich, A., Heyner, F.,, and Wendisch, M. (2013), Application of ground-based hyperspectral imaging to retrieve ice crystal shape and fields of cirrus optical thickness, Atmos. Meas. Tech. Discuss., 6, 1201–1238.

Schmidt, K. S., Pilewskie, P., Platnick, S., Wind, G., Yang, P., and Wendisch, M. (2007). Comparing irradiance fields derived from Moderate Resolution Imaging Spectroradiometer airborne simulator cirrus cloud retrievals with solar spectral flux radiometer measurements. J. Geophys. Res., 112:D24206, doi:10.1029/2007JD008711.

Siebert, H., Bethke, J., Conrath, T., Ditas, F., Hartmann, S., Katzwinkel, J., Schmeissner, T., Stratmann, F.,Wehner, B.,Wex, H., Shaw, R., Roberts, G., Nuijens, L., Stevens, B., Serikov, I., Ehrlich, A., Bierwirth, E., Schäfer, M., Wendisch, M., Werner, F., Izaguirre, M. A., and Farrell, D. (2012). The Fine-Scale Structure of the Trade Wind Cumuli over Barbados – An Introduction to the CARRIBA Project. Atmos. Chem. Phys. Discuss., 12, 28609-28660.

Wendisch, M., Müller, D., Schell, D., and Heintzenberg, J.: An airborne spectral Albedometer with active horizontal stabilization, J. Atmos. Ocean. Tech., 18, 1856–1866, 7757.

Wendisch, M., Pilewskie, P., Jäkel, E., Schmidt, S., Pommier, J., Howard, S., Jonsson, H. H., Guan, H., Schröder, M., and Mayer, B. (2004). Airborne measurements of areal spectral surface albedo over different sea and land surfaces. J. Geophys. Res., 109:D08203, doi:10.1029/2003JD004392.

Wendisch, M., Pilewskie, P., Pommier, J., Howard, S., Yang, P., Heymsfield, A. J., Schmitt, C. G., Baumgardner, D., and Mayer, B. (2005). Impact of cirrus crystal shape on solar spectral irradiance: A case study for subtropical cirrus. J. Geophys. Res., 110:D03202, doi:10.1029/2004JD005294.

Wendisch, M., Yang, P., and Pilewskie, P. (2007). Effects of ice crystal habit on thermal infrared radiative properties and forcing of cirrus. J. Geophys. Res., 112:D08201, doi:10.1029/2006JD007899.

Werner, F., Siebert, H., Pilewskie, P., Schmeissner, T., Shaw, R. A., and Wendisch, M. (2013), New airborne retrieval approach for trade wind cumulus properties under overlying cirrus, J. Geophys. Res., 118, doi:10.1002/jgrd.50 334.